Environmental Research 306 (2026) 125159

Contents lists available at ScienceDirect

Environmental Research

journal homepage: www.elsevier.com/locate/envres

Cord-blood black carbon particle burden is associated with a C19MC small extracellular vesicle miRNA signature enriched for neurodevelopmental pathways

Houman Kahroba [a,b,*], Kenneth Vanbrabant [b], Marcel van Herwijnen [a], Rick Kamps [a], Matthew Walker [c], Dagmar Waiblinger [c], Marcel Ameloot [d], Michelle Plusquin [b], John Wright [c], Tim Nawrot [b,e], Theo M. de Kok [a], Julian Krauskopf [a]

[a] Department of Translational Genomics, GROW Research Institute for Oncology and Reproduction, Maastricht University, Maastricht, the Netherlands
[b] Centre for Environmental Sciences, Hasselt University, Hasselt, Belgium
[c] Bradford Institute for Health Research, Bradford Teaching Hospitals NHS Foundation Trust, Bradford, UK
[d] Biomedical Research Institute, Hasselt University, Agoralaan Building C, Diepenbeek, 3590, Belgium
[e] School of Public Health, Occupational & Environmental Medicine, Leuven University, Leuven, Belgium

ARTICLE INFO

Keywords:
Combustion-derived particles
Size-exclusion chromatography
Pregnancy
Air pollution

ABSTRACT

Background: Ambient air pollution, particularly black carbon (BC), is associated with adverse pregnancy outcomes, but the molecular pathways linking *in utero* particle exposure to fetal programming remain incompletely understood. We examined whether cord-blood BC particle burden relates to small extracellular vesicle (sEV)-associated microRNA (miRNA) profiles and enriched developmental pathways.

Methods: Cord blood was collected from newborns in the Born in Bradford's Better Start (BiBBS) cohort. Plasma sEVs were isolated and miRNA was profiled by small RNA sequencing. BC particle load in whole cord blood was quantified by femtosecond pulsed-laser microscopy. After quality control and complete-case restriction, 68 newborns were included in the analysis. Candidate miRNAs were prioritised using elastic-net regression, and associations with $\log_{10}$-transformed BC particle burden were estimated using linear mixed-effects models with covariate adjustment and Benjamini---Hochberg false discovery rate (BH-FDR) control.

Results: Five of the ten candidate miRNAs were associated with BC at BH-FDR $\leq$0.10: hsa-miR-25-3p and hsa-miR-433-3p (positive associations) and hsa-miR-518a-3p, hsa-miR-519a-3p/519b-3p, and hsa-miR-520g-3p/520h (negative associations). Three of the five negatively associated miRNAs belong to the placenta-specific chromosome 19 miRNA cluster (C19MC). All five signals were robust in 100 $\times$ 20% holdout resampling. Validated target pathway analysis revealed enrichment for developmental and specifically neurodevelopmental processes, including axon guidance and neurotrophin signaling.

Conclusions: These findings link cord-blood BC particle burden to a placenta-linked C19MC miRNA signature in newborn sEVs and developmental pathway enrichment, providing molecular evidence consistent with particle-associated fetal programming at birth.

1. Introduction

Air pollution is a major environmental health risk, and ambient particulate matter (PM) exposure during pregnancy has been associated with adverse birth outcomes such as low birth weight and preterm birth (Bové et al., 2019). Black carbon (BC) is a carbonaceous component of PM produced by incomplete combustion (e.g. from traffic and biomass burning) and is considered particularly harmful due to its ability to carry toxic heavy metals and organic compounds on its surface (Janssen et al., 2011; Niranjan and Thakur, 2017). BC particles are typically ultrafine (<1 μm) and can translocate from the lungs into systemic circulation (Pope et al., 2006). Importantly, recent studies have shown that inhaled BC particles can cross the placenta and reach the fetus (Bové et al., 2019; Bongaerts et al., 2022). BC particles have been detected in human

* Corresponding author. Department of Translational Genomics, GROW Research Institute for Oncology and Reproduction, Maastricht University, Maastricht, the Netherlands.
E-mail addresses: h.kahroba@maastrichtuniversity.nl, houman.kahroba@uhasselt.be (H. Kahroba).

https://doi.org/10.1016/j.envres.2026.125159
Received 18 March 2026; Received in revised form 16 June 2026; Accepted 29 June 2026
Available online 2 July 2026

placental tissue and including in cord blood, correlating with maternal air pollution exposure (Bové et al., 2019; Bongaerts et al., 2022; Saenen et al., 2017). These findings establish internal BC load (e.g. in cord blood) as a direct biomarker of fetal exposure to combustion-derived pollution. However, the molecular and biological impacts of prenatal BC exposure on the developing fetus remain poorly understood.

Alterations in the fetal epigenome have been proposed as a key mechanism linking prenatal environmental exposures to adverse outcomes in later life (Klibaner-Schiff et al., 2025). Among epigenetic regulators, microRNAs (miRNAs) are of particular interest. miRNAs are small (~22 nt) non-coding RNAs that post-transcriptionally regulate gene expression, and they play crucial roles in embryonic and placental development (Ilekis et al., 2016; Bernstein et al., 2003; Alisch et al., 2007; Suh et al., 2010). There is evidence that prenatal air pollution exposure can dysregulate miRNA expression in placental tissue and fetal or newborn compartments, including cord blood (Tsamou et al., 2018). Epidemiological studies increasingly support a role for particulate air pollution in shaping fetal and maternal microRNA regulation. For example, higher maternal PM2.5 exposure has been linked to lower expression of the oncogenic miR-17/92 cluster in newborn cord blood (Tsamou et al., 2020), a cluster involved in normal development of the lungs and other organs (Lu et al., 2007). Beyond "free" circulating miRNAs, emerging evidence indicates that extracellular vesicles (EVs) respond dynamically to particulate exposures and may act as carriers of exposure-related signals: short-term PM exposure has been associated with increased circulating EV release and altered EV-packaged miRNA profiles in human panels, with downstream links to coagulation and cardiometabolic pathways (Bonzini et al., 2017; Pergoli et al., 2017). In pregnancy, PM exposure has been related to changes in total EV levels and placenta-derived (Syncytin-1^{+}) EVs, alongside EV-miRNA signatures consistent with inflammatory and hypertensive pregnancy pathways (Ferrari et al., 2022); similarly, maternal EV-miRNA patterns have been associated with multiple ambient and traffic-related air pollutants in a pregnancy cohort (Foley et al., 2024), and prenatal PM2.5 has been associated with placenta small-EV miRNAs in relation to infant neurodevelopment (Wang et al., 2022). Importantly, the biological plausibility for transplacental particulate effects is strengthened by direct visualization studies showing that BC particles reach the fetal side of the human placenta (Bové et al., 2019) and can be detected in cord blood and fetal organs in population-based studies (Bongaerts et al., 2022). Air pollution-induced changes in miRNA expression have also been observed in other contexts; experimental and human studies report that exposure to particulate matter can alter circulating miRNAs involved in inflammation and vascular function (Rodosthenous et al., 2015; Kahroba et al., 2025).

In pregnancy, the placenta is a key organ that may mediate fetal exposure and responses to pollutants. The human placenta expresses a unique set of miRNAs, including many clustered on chromosome 19 (the C19MC cluster), which are almost exclusively expressed in trophoblast cells and are secreted into the circulation via EVs (Jin et al., 2024). EVs are extracellular vesicles (~30-150 nm) released by cells, containing miRNAs, that facilitate intercellular communication. During pregnancy, placenta-derived EV-derived miRNAs enter maternal blood and can modulate maternal physiology (Xu et al., 2021). EV-derived miRNAs also circulate in the fetus (via cord blood), reflecting both placental and fetal tissue signals. These circulating miRNAs are stable (protected by vesicles) and thus attractive as accessible biomarkers of intrauterine conditions. Several placenta-specific miRNAs (including members of the C19MC cluster such as miR-518 and miR-519) have been implicated in pregnancy complications and fetal growth. For instance, altered expression of miR-518b and miR-519a in placental tissue is associated with intrauterine growth restriction (IUGR) and low birth weight (Wang et al., 2014), and elevated miR-519d levels have been noted in pre-eclampsia placentas (Cao et al., 2025). These findings underscore that dysregulation of placental miRNAs can adversely affect fetal development.

In summary, emerging evidence underscores the unique vulnerability of the developing fetus to maternal particulate exposure and highlights microRNAs as potential mediators of these effects. However, a critical knowledge gap remains in linking transplacental BC exposure with specific molecular responses in the fetus. In this study, we address this gap by integrating a quantitative biomarker of *in utero* BC exposure, cord blood BC particle load, with profiling of sEV-encapsulated microRNAs in newborn cord blood.

We aim to identify distinct EV-miRNA signatures that associate with BC exposure and that provides us with information of the molecular processes that are responsive to this exposure. Based on pathway analysis, we sought to identify biological pathways potentially linked to fetal developmental signaling, with particular attention to neurodevelopmental processes.

2. Materials and methods

2.1. Study population and sample collection

The analysis was embedded within the Born in Bradford's Better Start (BiBBS) birth cohort, in Bradford, UK. (Bridges et al., 2025; Dickerson et al., 2022) Eligibility for the parent BiBBS cohort required women to be registered to give birth at Bradford Royal Infirmary, to reside within the Better Start Bradford areas at the time of approach, and to provide consent during pregnancy or up to two weeks postpartum. Each eligible pregnancy during the recruitment period could contribute to the cohort, and all babies from the consented pregnancy, including multiple births, were eligible. Women were excluded from BiBBS if they planned to move out of the Better Start Bradford areas before birth. For the present molecular substudy, we further restricted the analysis to samples with available cord-blood plasma, cord-blood BC quantification, small-RNA sequencing data, and complete metadata required for the association analyses. Although multiple births were eligible in the parent BiBBS cohort, the present final analytic sample was restricted to singleton pregnancies; no multiple births were included among the 68 mother-infant dyads. Of the enrolled mother-infant dyads, 110 had complete, high-quality exposure and metadata; of these, 92 passed transcriptomic quality control (QC) and were retained for primary analyses. All participants provided written informed consent in line with the Declaration of Helsinki and institutional requirements (North West Research Ethics Committee 15/NW/0829; Leeds Bradford Research Ethics Committee 15/YH/0455). At enrolment, a structured questionnaire was used to collect information on demographics (maternal age, education, self-identified race/ethnicity) and lifestyle factors (including smoking during pregnancy). At delivery, approximately 10 mL of umbilical cord blood was collected into EDTA tubes and processed within 2 h; whole blood aliquots were stored at −80 °C for BC quantification and total cord blood RNA isolation. Plasma was separated by centrifugation and stored at −80 °C in the BiBBS biobank for EV isolation. The derivation of the final analytic sample is summarized in Fig. 1.

2.2. Small extracellular vesicle isolation and miRNA sequencing

For each participant, 250 μL of plasma was thawed on ice and processed using a standardized EV isolation workflow optimized for biofluids. Initially, sequential low-speed centrifugation steps were applied to remove cells and residual debris (300×g for 10 min, followed by 16,000×g for 20 min, both at 4 °C). The resulting clarified plasma was then subjected to a combined polymer-precipitation and size-exclusion chromatography (SEC) procedure. An appropriate volume of Exo-spin™ precipitation buffer (Cell Guidance Systems, EX02 kit) was added to the plasma, and samples were incubated on ice for 1 h according to the manufacturer's protocol. The concentrated material was subsequently applied to Exo-spin SEC columns pre-equilibrated with phosphate-buffered saline (PBS), and the flow-through fractions containing the majority of EVs were collected (Chandrasekera et al., 2023).

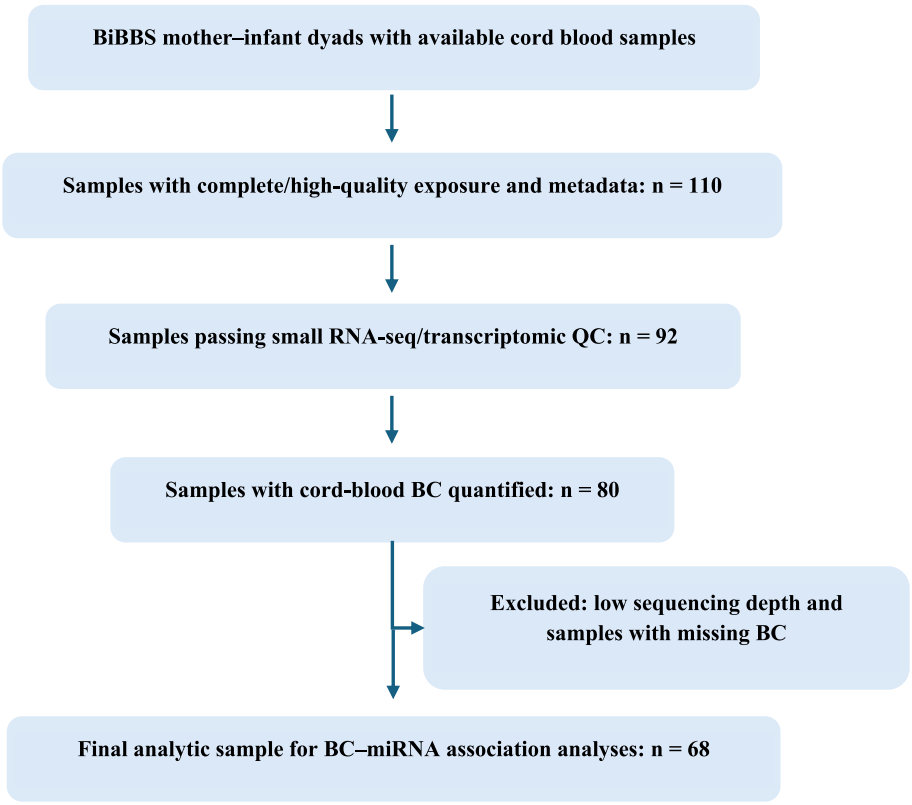

Fig. 1. Study flow diagram for the BiBBS cord-blood BC-miRNA analysis. Flow of mother-infant dyads from available cord-blood samples to the final analytic sample used for the black carbon (BC)-miRNA association analyses. Among BiBBS dyads with available cord-blood samples, 110 had complete/high-quality exposure and metadata. Of these, 92 passed small RNA-sequencing quality control, and 80 had cord-blood BC quantified. After excluding samples with low miRNA sequencing depth and incomplete data required for the BC-miRNA models, 68 mother-infant dyads remained in the final analytic sample. BC, black carbon; BiBBS, Born in Bradford's Better Start; miRNA, microRNA; QC, quality control.

The final EV preparation (180 μL) was stored at −80 °C until further analysis. All procedures were performed with RNAse-free, sterile consumables to minimize RNA contamination and degradation.

Total RNA was isolated from the EV preparations using the miRNeasy Serum/Plasma Advanced kit (Qiagen, Cat. no. 217204). Procedures followed the manufacturer's instructions. Agilent Bioanalyzer profiles (Small RNA chip) consistently demonstrated a broad small-RNA peak in the 20-40 nt range, compatible with miRNA-sized fragments. Small RNA libraries were generated using the NEXTFLEX Small RNA-Seq v4 kit with UDIs (PerkinElmer, cat. no. NOVA-5132-41). This protocol involves ligation of 3′ and 5′ adapters to small RNAs, cDNA synthesis, and PCR amplification with barcoded primers. We used the maximum possible RNA input (4 μL of eluate, estimated <5 ng total RNA). Adapter ligation was carried out at 25 °C for 1 h for the 3′ adapter and 16 °C for 1 h for the 5′ adapter, using the kit's proprietary ligases. Reverse transcription was then performed, followed by PCR amplification (25 cycles, as recommended for low-input material). Unique dual indices were assigned to each sample to enable multiplexing. Libraries were size-selected with magnetic beads to enrich inserts corresponding to 15-35 nt RNAs (resulting in a final library size of ~145 bp including adapters). Library size distribution and integrity were assessed on a Bioanalyzer High Sensitivity DNA chip (Cat. no. 5067-4626). Libraries were quantified, normalized, and pooled in equimolar amounts. Sequencing was performed on an Illumina NovaSeq platform, generating single-end 75 nt reads.

2.3. Cord blood black carbon measurement

BC particle concentration in whole cord blood was quantified using the Hasselt University label-free femtosecond pulsed-laser microscopy approach based on non-incandescence-related white-light (WL) generation by carbonaceous particles (Bové et al., 2016). Cord blood was collected in plastic EDTA tubes and stored frozen (−80 °C) until analysis; after minimal thawing, aliquots were mounted in sealed imaging chambers (24 × 24 mm; nominal thickness ~0.17 mm) (Bongaerts et al., 2022). Samples were scanned on a multiphoton laser-scanning microscope (e.g., Zeiss LSM880) under femtosecond near-infrared excitation (commonly 810 nm, 80 MHz; ~5-10 mW at the specimen) (Bové et al., 2016). BC particles were identified operationally by two WL characteristics: (i) an extremely bright signal that readily saturates compared with endogenous label-free signals and (ii) broadband emission spanning the visible spectrum; therefore, particles were detected by applying intensity thresholds and retaining only supra-threshold signals concurrently present in both acquisition channels (e.g., SHG 400-410 nm and TPAF 450-650 nm) (Bové et al., 2019; Bongaerts et al., 2022). Particle counts were quantified via an automated image-analysis workflow and expressed as number of particles per milliliter of cord blood.

2.4. Bioinformatics and statistical analysis

Raw sequencing reads were adapter-trimmed and quality-filtered prior to alignment and quantification using miRge3.0. Processed reads were aligned to human mature miRNA reference sequences from miRBase v22 to quantify known miRNAs, generating a per-sample mature-miRNA count matrix. All downstream analyses were conducted in R v4.1. For sequencing-depth reporting, raw total sequencing reads were used as the denominator. The proportion of reads assigned to annotated mature miRNAs was calculated as total mature-miRNA counts divided by raw total sequencing reads.

The analytic set comprised 92 cord-blood samples with high-quality

small RNA-seq data and clinical metadata; cord-blood BC was quantified in 80 of these using femtosecond pulsed-laser microscopy. After excluding libraries with extremely low sequencing depth, defined a priori as total miRNA counts <20% of the cohort median (<45,190 total miRNA counts; cohort median = 225,952; 13 libraries excluded), and samples with missing BC measurements, 68 mother-infant pairs were retained for association analyses.

The miRNA count data were processed using DESeq2 (Love et al., 2014). A DESeq data set was created with an intercept-only design (~1) and used to estimate size factors and dispersions for normalization and quality control. miRNAs with <10 total reads across all retained samples were removed prior to downstream QC. For global QC and exploratory analyses, we required miRNAs to have ≥3 raw counts in ≥30% of libraries and applied the variance-stabilizing transformation (VST; blind = TRUE). Library size distributions, dispersion trends, and VST-based principal component analysis (PCA) were examined by infant sex, maternal ethnicity, RNA batch, and quartiles of log10-transformed cord-blood BC to identify outliers and potential batch effects.

We applied additional feature-level filtering to retain robust, informative miRNAs. Starting from the VST matrix of QC-passed miRNAs, we retained miRNAs that (i) were "detected" (raw counts ≥3) in at least 40% of samples, (ii) showed limited floor effects (≤30% of samples within ±0.05 VST units of the miRNA-specific baseline estimated from zero-count observations), and (iii) demonstrated sufficient variability (VST standard deviation ≥ 25th percentile across miRNAs). This produced the final modelling matrix.

To screen for BC-associated miRNAs, we first applied elastic-net regression using glmnet (Gaussian family; $\alpha = 0.1$). The outcome was log10(BC per mL) and predictors were filtered VST miRNA expression values (samples × miRNAs). Penalization was guided by up to 10-fold cross-validation (limited by sample size), and the final penalty was set to $\lambda = 0.7 \times \lambda\_min$. This slightly relaxed penalty was chosen a priori for candidate screening because cord-blood sEV miRNAs are biologically correlated, and a stricter penalty can select an overly sparse set in small datasets. The elastic-net step was used only for dimensionality reduction and candidate prioritization, not for formal statistical inference. miRNAs with non-zero coefficients at this λ (excluding the intercept) were carried forward.

For each elastic-net-selected miRNA, we then fitted per-miRNA regression models with VST expression as the dependent variable and log10(BC per mL) as the primary exposure. Models included the fixed-effect covariates infant sex, maternal ethnicity, and maternal age at delivery. Maternal smoking during pregnancy was considered as a covariate but was not included in the primary models because it was self-reported and incomplete, which would reduce sample size and increase the risk of selection bias. Given the modest sample size, we used a parsimonious adjustment set. Cord-blood BC is a directly measured internal biomarker integrating combustion-related particle exposure from multiple sources, including potential tobacco-related particulate exposure. However, smoking may still influence miRNA expression through broader systemic mechanisms not fully captured by measured BC burden, such as inflammatory, oxidative stress-related, vascular, placental, and metabolic effects. RNA sequencing batch was included as a random intercept. Because the per-miRNA models were fitted after penalized candidate selection, the resulting p-values are post-selection and were interpreted descriptively rather than as confirmatory hypothesis tests. We therefore emphasized nominal p-values among the 10 elastic-net-selected candidates and reported Benjamini-Hochberg FDR values for transparency. To assess robustness, we implemented a 100 × 20% hold-out procedure restricted to the FDR ≤0.10 candidate set. In each iteration, 20% of samples were randomly excluded, models were refit in the remaining 80%, and the BC coefficients were stored. Coefficient distributions across iterations were summarized graphically to evaluate stability of effect direction and magnitude for each candidate miRNA.

Experimentally validated miRNA-target interactions for the selected miRNAs were retrieved using the multiMiR R package, which integrates curated miRNA-target resources; analyses were restricted to experimentally supported interactions (e.g., miRTarBase and DIANA-TarBase) to avoid reliance on purely in silico target prediction. Target genes were mapped to Entrez Gene IDs using the human annotation package org.Hs.eg.db, and the background ("gene universe") for over-representation analysis (ORA) was defined as all Entrez IDs available in org.Hs.eg.db. ORA was performed in R using clusterProfiler: GO Biological Process (GO-BP) enrichment was computed with enrichGO (Gene Ontology), and KEGG pathway enrichment with enrich KEGG (Kyoto Encyclopedia of Genes and Genomes). Enrichment p-values were adjusted for multiple testing using the Benjamini-Hochberg false discovery rate (FDR), and terms with FDR ≤0.05 were considered significant.

To focus interpretation on developmental biology, we implemented a predefined developmental subset filtering step for both GO-BP and KEGG outputs. For GO-BP, "developmental" terms were defined a priori as the Gene Ontology term GO:0032502 ("developmental process") and all of its GO-BP descendants (offspring terms) obtained from the GO ontology using GO.dbGOBPOFFSPRING. Significant GO-BP enrichment results were filtered to this descendant set and visualized as dot plots. For KEGG, to avoid conflating "developmental relevance" with broad disease pathway maps, we defined a curated disease-free developmental KEGG set capturing canonical developmental signaling and neurodevelopmental modules (Wnt, Notch, Hedgehog, TGF-β, Hippo, pluripotency signaling, axon guidance, neurotrophin signaling, synaptic vesicle cycle, and major synapse pathways). Significant KEGG enrichment results were filtered to this curated set and visualized as dot plots. GO redundancy was reduced with rrvgo by clustering semantically similar GO terms (method "Rel", threshold 0.7) and selecting a representative parent term per cluster. A miRNA × module matrix of -log10 (FDR) (0 = non-significant) was visualized as a heatmap using ComplexHeatmap, with a perceptually uniform viridis/cividis palette.

Reactome pathway enrichment was performed using ReactomePA as a supportive curated pathway analysis. GO-BP was considered the primary pathway database because developmental and neurodevelopmental terms could be defined objectively using ontology structure. As an additional sensitivity analysis, we tested whether developmental and neurodevelopmental GO-BP terms were over-represented among significant enriched GO-BP terms. Developmental terms were defined a priori as GO:0032502 ("developmental process") and all of its GO-BP descendant terms obtained using GO.db. Neurodevelopmental terms were defined as GO:0007399 ("nervous system development") and all of its GO-BP descendant terms. Fisher's exact test was used to compare the proportion of developmental or neurodevelopmental terms among significant GO-BP enrichment results with their proportion among all tested GO-BP terms. This analysis was interpreted as supportive because GO terms are hierarchically related and not statistically independent.

3. Results

3.1. Participant characteristics and exposure levels

The final analytic sample comprised 68 mother-infant pairs used for BC-miRNA association analyses (Table 1). Maternal age at delivery was 32.8 ± 5.1 years (median 32.0; IQR 29.0-36.0; n = 61). Birth weight was 3.21 ± 0.43 kg (median 3.17; IQR 2.97-3.48; n = 45). Infant sex was balanced, with 34 females and 34 males. The largest maternal ethnicity groups were Pakistani (38.2%) and White British (19.1%); maternal ethnicity was missing for 13 participants (19.1%). The median cord-blood BC concentration was 2.07×10^6 particles/mL (IQR 1.07×10^6-4.68×10^6; range 4.68×10^5-3.31×10^7). On the log10 scale, mean cord-blood BC was 6.38 ± 0.41 log10(particles/mL).

Table 1
Characteristics of the final analytic sample used for BC-miRNA association analyses. Gestational age, detailed pregnancy-related complications, and additional socioeconomic indicators were not available with sufficient completeness and reliability in the molecular substudy dataset, partly because sampling and data extraction overlapped with the COVID-19 period. These variables were therefore not included in the descriptive table or used as covariates.

Characteristic	Final analytic sample (n = 68)	Available
Maternal age at delivery, years	32.8 ± 5.1; median 32.0 (IQR 29.0–36.0)	61
Birth weight, kg	3.21 ± 0.43; median 3.17 (IQR 2.97–3.48)	45
Infant sex, n (%)		68
Female	34 (50.0)	
Male	34 (50.0)	
Maternal ethnicity, n (%)		68
Pakistani	26 (38.2)	
White British	13 (19.1)	
African	7 (10.3)	
Indian	3 (4.4)	
Bangladeshi	2 (2.9)	
Other/mixed	4 (5.9)	
Missing	13 (19.1)	
Cord-blood BC, particles/mL	Median 2.07×10^6 (IQR 1.07×10^6–4.68×10^6; range 4.68×10^5–3.31×10^7)	68
Log10 cord-blood BC, log10(particles/mL)	6.38 ± 0.41; median 6.32 (IQR 6.03–6.67; range 5.67–7.52)	68

3.2. Small extracellular vesicles characterization

We isolated EVs from 250 μL of umbilical cord blood plasma for each newborn. Vesicle enrichment and morphology were assessed using multiple complementary approaches in accordance with MISEV2023 recommendations (Welsh et al., 2024). First, overall sEV yield and basic characteristics were evaluated (Fig. 2). Nanoparticle tracking analysis (NTA) of total plasma sEVs showed a unimodal size distribution with a peak around 100 nm and particle concentrations within the expected range for plasma-derived vesicles (Fig. 2A). Cryogenic transmission electron microscopy (cryo-TEM) demonstrated intact, round, lipid bilayer-enclosed vesicles with diameters of approximately 30-150 nm (Fig. 2B), consistent with previously described EV morphology. Western blot analysis of total sEV preparations detected the canonical EV-derived markers CD9, CD63 and CD81 (Fig. 2C, (see Supplementary File S1 for full results), supporting the vesicular nature and EV-enriched profile of our isolates (Welsh et al., 2024).

3.3. Black carbon-associated EV-derived miRNAs

In the final BC-miRNA analytic sample, the median raw total sequencing depth was 79,640,000 reads per sample (IQR 67,765,000-96,045,000; range 17,720,000–139,930,000). Based on the mature-miRNA count matrix, samples yielded a median of 255,617 reads assigned to annotated mature miRNAs per sample (IQR 142,271-692,374; range 56,394–2,657,324), corresponding to a median of 0.40% of raw total sequencing reads assigned to annotated mature miRNAs (IQR 0.21-0.78%; range 0.08-3.90%). This relatively low percentage is consistent with the low abundance of miRNAs in cord-blood sEV/exosomal RNA preparations and the presence of other small-RNA fragments, non-miRNA reads, and possible adapter-derived reads in low-input EV small-RNA libraries (Wang et al., 2023). In the complete final analytic sample, a median of 341 miRNAs per sample were detected at raw count >0 (IQR 220-403; range 110-533), and a median of 339 miRNAs were detected at raw count ≥3 (IQR 220-403; range 109-531). Across the full count matrix, 1013 distinct miRNAs were observed.

After QC filtering, elastic-net screening retained 10 candidate miRNAs with non-zero coefficients: hsa-miR-433-3p, hsa-miR-518a-3p, hsa-miR-519a-3p/519b-3p, hsa-miR-148b-3p, hsa-miR-25-3p, hsa-miR-126-3p, hsa-miR-29a-3p, hsa-miR-497-5p, hsa-miR-520g-3p/520h, and hsa-miR-425-3p. In covariate-adjusted mixed-effects models, five of these candidates showed nominal associations with log10-transformed cord-blood BC: hsa-miR-25-3p ($\beta = 0.629$, $p = 0.0049$, BH-FDR = 0.049), hsa-miR-433-3p ($\beta = 0.639$, $p = 0.0186$, BH-FDR = 0.073), hsa-miR-518a-3p ($\beta = -0.603$, $p = 0.0272$, BH-FDR = 0.073), hsa-miR-519a-3p/519b-3p ($\beta = -0.944$, $p = 0.0293$, BH-FDR = 0.073), and hsa-miR-520g-3p/520h ($\beta = -0.522$, $p = 0.0397$, BH-FDR = 0.079; Fig. 3). Given the post-selection nature of the analysis, nominal p-values are emphasized and BH-FDR values are reported descriptively (Fig. 3).

In the 100 × 20% holdout analysis, these five miRNAs maintained consistent effect directions and coefficients centered close to the full-sample estimates (Fig. 4). The five miRNAs were detected at raw counts ≥3 in a high proportion of samples, ranging from 75.9% for hsa-miR-518a-3p to 98.7% for hsa-miR-25-3p, with a median detection fraction of 88.6%. These results support sampling stability of the exploratory BC-associated panel, although external replication remains necessary.

3.4. Pathway enrichment analysis of experimentally validated miRNA targets

To interpret the biological context of the BC-associated sEV-miRNAs, we performed over-representation analysis using experimentally

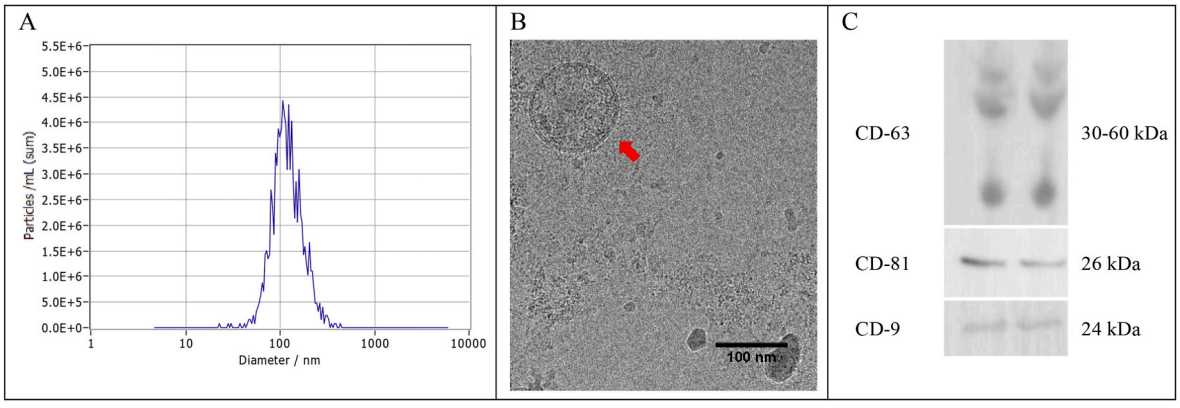

Fig. 2. Characterization of cord blood plasma-derived small extracellular vesicles (sEVs). (A) Nanoparticle tracking analysis (NTA) of the isolated vesicle fraction showing a predominant particle size mode at ~100 nm. (B) Representative cryo-transmission electron micrograph illustrating round, membrane-delimited vesicles (red arrow); scale bar, 100 nm. (C) Western blot detection of canonical EV-associated markers in the isolate: CD9 (~24 kDa), CD81 (~26 kDa), and CD63 (glycosylated smear ~30-60 kDa). (For interpretation of the references to color in this figure legend, the reader is referred to the Web version of this article.)

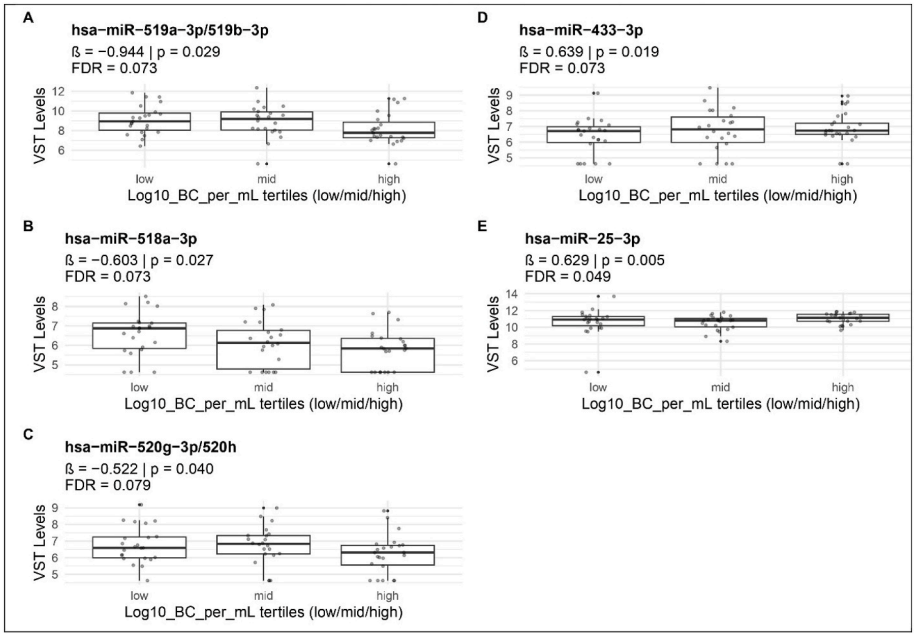

Fig. 3. Stable miRNAs across black carbon exposure tertiles. Box-and-whisker plots show variance-stabilizing transformed (VST) miRNA expression levels in samples grouped by Log10-BC per milliliter (mL) tertiles (low/mid/high) for visualization. Boxes indicate the interquartile range (IQR) with the median as the center line; whiskers extend to 1.5× IQR and points represent individual observations. Regression results are annotated per panel as β, nominal p, and FDR: (A) hsa-miR-519a-3p/519b-3p, (B) hsa-miR-518a-3p, (C) hsa-miR-520g-3p/520h (negative β), and (D) hsa-miR-433-3p, (E) hsa-miR-25-3p (positive β).

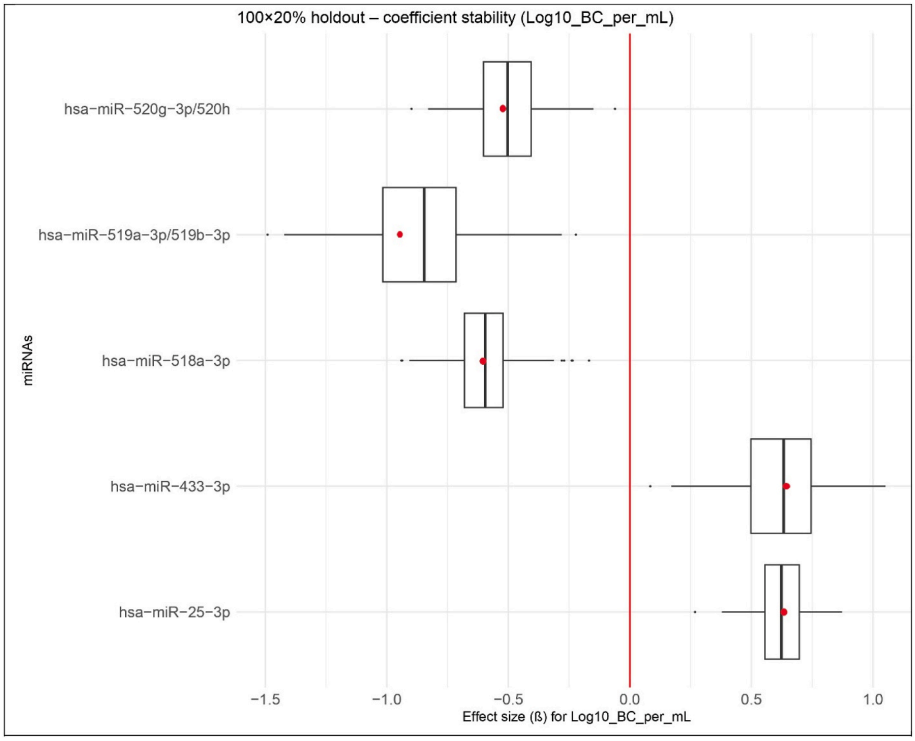

Fig. 4. Stability of black carbon-miRNA associations under repeated holdout resampling. Boxplots show the distribution of linear mixed-effects model β coefficients for the association between log10 cord-blood black carbon (BC; particles/mL) and cord-blood sEV-miRNA expression (VST scale) across 100 iterations of a 20% holdout procedure. In each iteration, models were refitted after randomly excluding 20% of the analytic samples. The horizontal dashed line denotes the null effect ($\beta = 0$). The large red circle indicates the full-sample mixed-effects model estimate. Positive β values indicate higher sEV-miRNA expression with higher BC, whereas negative β values indicate lower expression with higher BC. Boxes represent the interquartile range, center lines indicate the median, whiskers extend to 1.5× IQR, and points indicate outlying holdout estimates. (For interpretation of the references to color in this figure legend, the reader is referred to the Web version of this article.)

validated miRNA-target interactions retrieved from multiMiR. After mapping to Entrez identifiers, the combined validated target set of the five BC-associated miRNA signals comprised 8216 unique target genes. Because miRNA target databases are annotation-dense and may be

biased toward well-studied miRNAs and genes, we treated the pathway results as hypothesis-generating and used GO Biological Process (GO-BP) as the primary ontology-based analysis, with KEGG and Reactome as supportive curated pathway resources.

In the unrestricted GO-BP analysis, 1912 terms were enriched at BH-FDR ≤0.05 (Supplementary file S2). The strongest enriched terms reflected broad regulatory and intracellular processes, including small GTPase-mediated signal transduction (GO:0007264; BH-FDR = 1.43×10^{-20}), Golgi vesicle transport (GO:0048193; BH-FDR = 5.23×10^{-20}), regulation of protein catabolic process (GO:0042176; BH-FDR = 5.23×10^{-20}), proteasome-mediated ubiquitin-dependent protein catabolic process (GO:0043161; BH-FDR = 7.07×10^{-19}), and regulation of neuron projection development (GO:0010975; BH-FDR = 7.07×10^{-19}). These results indicate that the validated targets of the BC-associated miRNAs are enriched for broad regulatory, transport, protein-turnover, and cell-signaling processes.

To focus on developmental biology, we next filtered the GO-BP results using the predefined GO:0032502 "developmental process" branch and all of its descendant terms (Fig. 5A and Supplementary file S3). This identified 386 developmental GO-BP terms at BH-FDR ≤0.05. The strongest developmental terms included regulation of neuron projection development (GO:0010975; BH-FDR = 7.07×10^{-19}), axonogenesis (GO:0007409; BH-FDR = 2.24×10^{-15}), *in utero* embryonic development (GO:0001701; BH-FDR = 7.99×10^{-15}), regulation of nervous system development (GO:0051960; BH-FDR = 1.29×10^{-14}), and regulation of neurogenesis (GO:0050767; BH-FDR = 4.39×10^{-13}). Additional enriched terms included developmental growth involved in morphogenesis, synapse assembly, dendrite development, telencephalon development, and forebrain development.

Because pathway enrichment analyses can be influenced by the composition of the tested pathway background, we performed a GO-BP sensitivity analysis using Fisher's exact test. Developmental GO-BP terms were not formally over-represented among significant enriched GO-BP terms compared with the tested GO-BP background (odds ratio = 1.07, 95% CI = 0.96-∞, p = 0.157). In contrast, neurodevelopmental GO-BP terms, defined as GO:0007399 "nervous system development" and all descendant terms, were significantly over-represented among significant enriched GO-BP terms (odds ratio = 1.50, 95% CI = 1.21-∞, p = 7.81×10^{-4}). Specifically, 111 neurodevelopmental GO-BP terms were significant at BH-FDR ≤0.05, corresponding to 5.8% of significant GO-BP terms compared with 3.9% of non-significant GO-BP terms. This supports the interpretation that the neurodevelopmental signal was not solely driven by the overall frequency of neurodevelopmental annotations among tested GO-BP terms (Supplementary file S4).

Supportive KEGG analysis showed concordant enrichment of canonical developmental and neurodevelopmental pathways (Fig. 5B and Supplementary file S5). In the curated disease-free developmental KEGG subset, all 13 predefined pathways were enriched at BH-FDR ≤0.05. The strongest pathways were axon guidance (hsa04360; BH-FDR = 2.53×10^{-9}), neurotrophin signaling pathway (hsa04722; BH-FDR = 9.88×10^{-9}), Hippo signaling pathway (hsa04390; BH-FDR = 9.88×10^{-9}), Wnt signaling pathway (hsa04310; BH-FDR = 2.51×10^{-7}), and TGF-beta signaling pathway (hsa04350; BH-FDR = 8.14×10^{-7}). Additional enriched pathways included signaling pathways regulating pluripotency of stem cells, dopaminergic synapse, glutamatergic synapse, cholinergic synapse, synaptic vesicle cycle, Notch signaling pathway, GABAergic synapse, and Hedgehog signaling pathway.

General KEGG and Reactome analyses supported the broader regulatory interpretation but were not used as the primary basis for developmental inference (Supplementary file S6 and S7, respectively). General KEGG analysis identified 177 enriched pathways at BH-FDR ≤0.05, including focal adhesion, endocytosis, nucleocytoplasmic transport, protein processing in the endoplasmic reticulum, autophagy, and cell cycle. Reactome analysis identified 656 enriched pathways at BH-FDR ≤0.05, with top terms including RHO GTPase cycle, signal transduction by growth factor receptors and second messengers, capped intron-containing pre-mRNA processing, intracellular signaling by second messengers, SUMOylation, M phase, and TGF-beta receptor signaling. Together, these results indicate that BC-associated sEV-miRNAs target broad intracellular regulatory networks, with a reproducible and statistically supported enrichment of neurodevelopmental GO-BP annotations.

3.5. MicroRNA-specific enrichment patterns

To gain more granular insight, we next examined pathway enrichment results for each BC-associated miRNA individually (validated targets only; developmental GO-BP/KEGG libraries; Fig. 6 and Supplementary File S8). Despite originating from distinct genomic loci and having partially non-overlapping target sets, these miRNAs showed convergent enrichment of developmental themes, with the strongest convergence on neurodevelopmental programs.

Among the up-regulated miRNAs, miR-25-3p exhibited extremely strong enrichment for broad neurodevelopmental processes, including neurogenesis (GO:0022008; q = 3.61×10^{-39}; fold enrichment = 1.40), generation of neurons (GO:0048699; q = 8.59×10^{-36}; fold enrichment = 1.41), and regulation of neuron projection development (GO:0010975; q = 4.07×10^{-17}; fold enrichment = 1.54). These results suggest that higher miR-25-3p in high-BC newborns could plausibly bias signaling toward relative suppression of neuronal differentiation/neurite outgrowth gene programs (hypothesis-generating, consistent with the breadth of its mapped validated target set). Similarly, miR-433-3p (also up-regulated) showed robust enrichment across neurodevelopmental terms, including neurogenesis (GO:0022008; q = 3.55×10^{-15}; fold enrichment = 2.03) and generation of neurons (GO:0048699; q = 2.84×10^{-14}; fold enrichment = 2.08), alongside significant enrichment for heart development (GO:0007507; q = 0.00129; fold enrichment = 1.81). Together, these findings indicate that multiple up-regulated BC-responsive EV-miRNAs converge on gene networks central to nervous system development, with additional signals extending to cardiac developmental pathways.

Interestingly, the placenta-associated C19MC miRNAs responded in the opposite direction (miR-518a-3p and miR-519a-3p/miR-519b-3p were down-regulated with higher BC), yet their validated target enrichment still mapped to developmental programs. Both miR-519a-3p and miR-519b-3p showed significant enrichment for neurodevelopmental processes at FDR <0.05, including neurogenesis (miR-519a-3p: q = 7.0×10^{-5}; fold enrichment = 1.88; miR-519b-3p: q = 4.06×10^{-4}; fold enrichment = 1.78) and regulation of axonogenesis (miR-519a-3p: q = 5.55×10^{-4}; fold enrichment = 4.39; miR-519b-3p: q = 0.00263; fold enrichment = 4.08), indicating that these trophoblast-enriched miRNAs plausibly participate in regulating neurodevelopment-related gene networks. This is biologically plausible because C19MC miRNAs are highly enriched in human trophoblasts and are abundant in trophoblast-derived exosomes, supporting a mechanistic link between placental EV-miRNA signaling and fetal developmental pathways (Donker et al., 2012; Ouyang et al., 2013).

Also, miR-518a-3p showed significant developmental enrichments at FDR <0.05, including neurogenesis (GO:0022008; q = 0.01281; fold enrichment = 1.67), T cell differentiation in thymus (GO:0033077; q = 0.01547; fold enrichment = 5.09), and osteoblast differentiation (GO:0001649; q = 0.01770; fold enrichment = 3.03). Given that miR-518a-3p was down-regulated, the directionality framework predicts relative activation of these gene programs via derepression of validated targets, again, best interpreted as a data-driven hypothesis that connects placental EV-miRNA shifts with fetal developmental signaling.

Hsa-miR-520h (C19MC-adjacent; negatively associated with BC) showed robust developmental enrichment among experimentally validated targets (developmental subset; BH-FDR ≤0.05). The strongest signals clustered around cardiovascular morphogenesis and

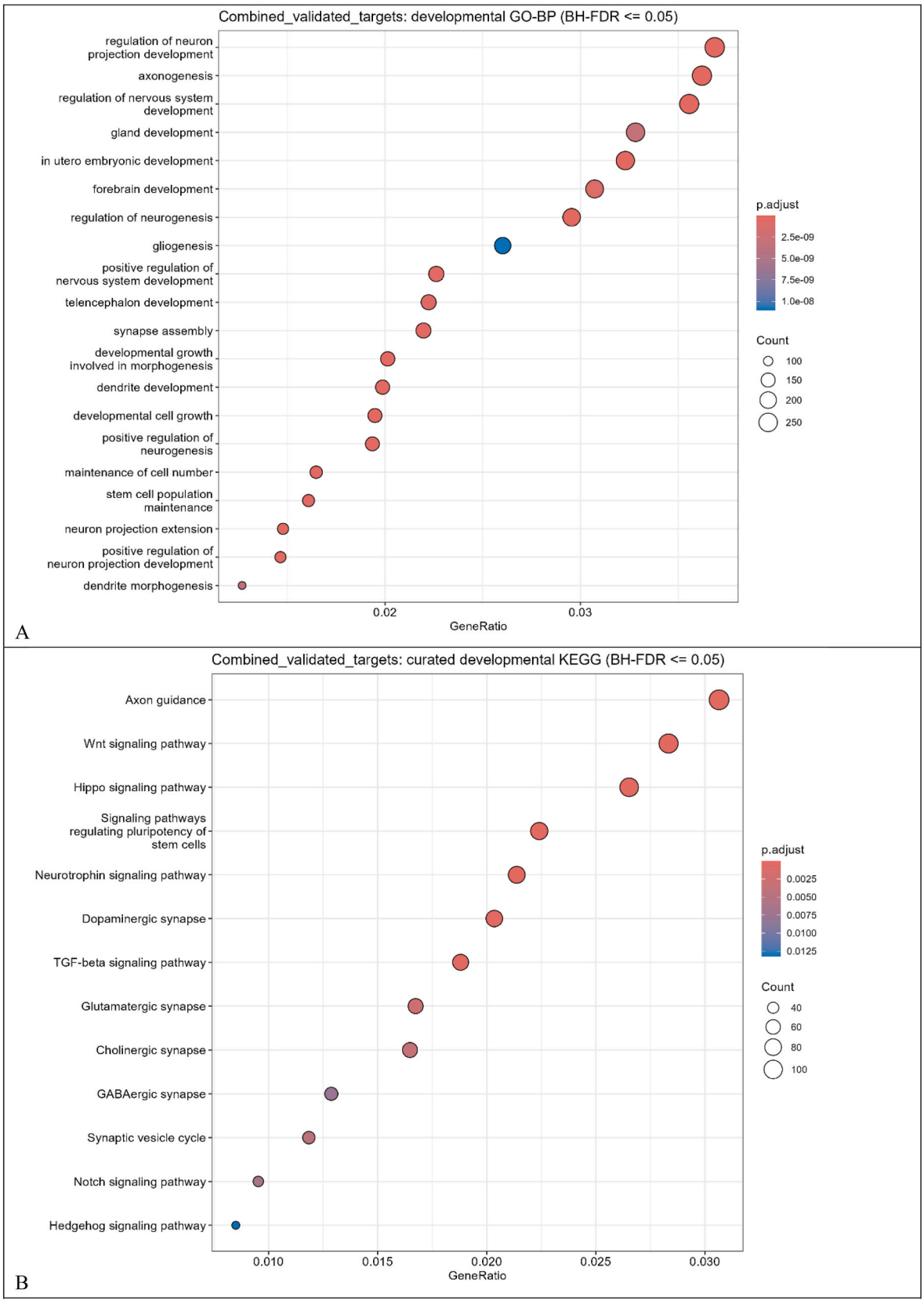

(caption on next page)

Fig. 5. Fig. 5A. **Developmental GO Biological Process enrichment among validated targets of BC-associated sEV-miRNAs.** Dot plot showing enriched Gene Ontology Biological Process (GO-BP) developmental terms among experimentally validated target genes of the five black carbon (BC)-associated sEV-miRNA signals. Terms were restricted to the predefined GO:0032502 "developmental process" branch and its descendant terms. Only terms passing Benjamini–Hochberg false discovery rate correction (BH-FDR ≤0.05) are shown. The x-axis shows the GeneRatio, defined as the proportion of validated target genes annotated to each GO-BP term. Dot size represents the number of target genes contributing to each term, and dot color indicates the adjusted p-value. The enrichment pattern highlights neurodevelopmental processes, including regulation of neuron projection development, axonogenesis, regulation of nervous system development, regulation of neurogenesis, synapse assembly, dendrite development, telencephalon development, and forebrain development. (B) Curated developmental KEGG pathway enrichment among validated targets of BC-associated sEV-miRNAs.Dot plot showing enriched curated developmental and neurodevelopmental KEGG pathways among experimentally validated target genes of the five black carbon (BC)-associated sEV-miRNA signals. The KEGG results were filtered to a predefined disease-free developmental pathway set, including canonical morphogen signaling, pluripotency, axon guidance, neurotrophin signaling, synaptic vesicle cycling, and major synaptic pathways. Only pathways passing Benjamini–Hochberg false discovery rate correction (BH-FDR ≤0.05) are shown. The x-axis shows the GeneRatio, defined as the proportion of validated target genes annotated to each KEGG pathway. Dot size represents the number of target genes contributing to each pathway, and dot color indicates the adjusted p-value. The enriched pathways highlight axon guidance, Wnt, Hippo, TGF-beta, Notch, Hedgehog, neurotrophin signaling, pluripotency signaling, and synaptic pathways, supporting the GO-BP-based neurodevelopmental enrichment results. (For interpretation of the references to color in this figure legend, the reader is referred to the Web version of this article.)

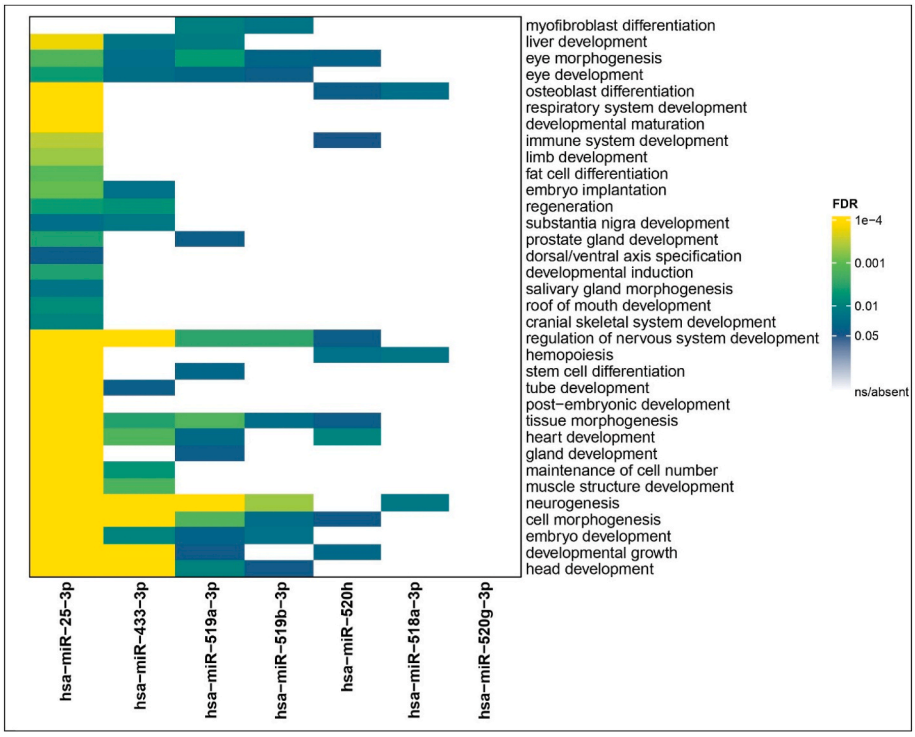

Fig. 6. GO:BP and KEGG module-level enrichment summary across miRNAs (validated evidence; FDR ≤ 0.05). Significant GO Biological Process and KEGG terms (BH-FDR ≤0.05) were first reduced for redundancy by grouping semantically similar GO terms into modules using rrvgo, which clusters terms based on a semantic similarity matrix and selects a representative term per cluster. The heatmap displays, for each miRNA (columns) and module (rows), the most significant term mapped to that module; color represents, -log10(BH-FDR), so higher intensity corresponds to stronger enrichment (smaller FDR), and white indicates non-significant or absent enrichment. (For interpretation of the references to color in this figure legend, the reader is referred to the Web version of this article.)

hematopoietic/immune differentiation, with additional regulation of growth and neurodevelopment. Specifically, enriched GO-BP terms included heart development (GO:0007507; $q = 7.81 \times 10^{-3}$), myeloid cell differentiation (GO:0030099; $q = 1.70 \times 10^{-2}$), and regulation of developmental growth (GO:0048638; $q = 2.32 \times 10^{-2}$). More granular cardiac processes were also significant, including cardiac ventricle development (GO:0003231; $q = 2.88 \times 10^{-2}$) and ventricular septum development (GO:0003281; $q = 2.88 \times 10^{-2}$). Finally, regulation of neurogenesis remained significant (GO:0050767; $q = 4.06 \times 10^{-2}$). Given that miR-520h was down-regulated with higher BC, the enrichment pattern is directionally consistent with de-repression of target genes and predicted activation of these cardiac/hematopoietic/growth programs. These findings are consistent with prior reports showing that placenta-enriched C19MC miRNAs are packaged into trophoblast-derived extracellular vesicles and participate in maternal-fetal communication. This supports a plausible placental EV-mediated route through which changes in C19MC miRNA abundance could be linked to fetal developmental signaling (Donker et al., 2012; Ouyang et al., 2013).

Finally, hsa-miR-520g-3p did not yield significant developmental enrichment at FDR <0.05, however, when relaxing the threshold to FDR <0.10, miR-520g-3p showed borderline developmental/lineage signals, including regulation of osteoclast differentiation (GO:0045670; q = 0.0585; fold enrichment = 4.33), myeloid cell differentiation (GO:0030099; q = 0.0601; fold enrichment = 2.08), axis specification (GO:0009798; q = 0.0711; fold enrichment = 3.59), stem cell population maintenance (GO:0019827; q = 0.0726; fold enrichment = 2.75), and vascular/cardiac terms such as vasculogenesis (GO:0001570; q = 0.0852; fold enrichment = 3.76) and heart development (GO:0007507; q = 0.0852; fold enrichment = 1.83). Because miR-520g-3p was down-regulated, these borderline enrichments are directionally consistent with predicted activation of hematopoietic/stem/vascular programs via derepression, although the relaxed FDR warrants cautious interpretation.

Fig. 6 provides a comparative overview of selected developmental

pathway enrichments for each miRNA. Although these BC-associated EV-miRNAs originate from distinct loci and have different validated target sets, they collectively converge on developmental pathways, most consistently neurodevelopment, with additional signals involving cardiac, vascular, and hematopoietic/immune differentiation. These results suggest that prenatal combustion-derived particulate exposure may influence developmental gene-regulatory trajectories through EV-miRNA-associated signaling, although direct functional validation is still needed. Full per-miRNA developmental enrichment results (validated targets) are provided in Supplementary File S8, and the per-miRNA general pathway analysis is available in Supplementary File S9.

4. Discussion

This study is the first to demonstrate an association between cord-blood BC particle burden, a directly measured biomarker of prenatal transplacental particle exposure, and altered EV-associated microRNA profiles in newborn cord blood at delivery. We identified a panel of cord blood EV-miRNAs whose expression levels were related to transplacental BC particle load, and we found that these miRNAs collectively target genes enriched in critical developmental pathways. Our findings shed new light on molecular mechanisms that may underlie the epidemiological links between prenatal air pollution and adverse birth outcomes (Bové et al., 2019; Ji et al., 2023). In particular, the enrichment of neurodevelopmental, cardiovascular, and placental signaling pathways among the targets of BC-associated miRNAs provides a plausible biological bridge connecting maternal exposure to combustion-derived pollutants with fetal developmental signaling.

Several of the identified miRNAs have known roles in regulating cell proliferation, differentiation, and survival, suggesting that their dysregulation could affect fetal development. miR-25-3p is part of the conserved miR-106b∼25 cluster, a member of the broader miR-17∼92 family of developmental microRNA clusters that help tune proliferation, differentiation, and survival programs during embryonic and fetal growth (Concepcion et al., 2012). Functionally, miR-25/miR-106b∼25 activity aligns with "growth-phase" biology: in the developing/early postnatal heart, the cluster (including miR-25) promotes cardiomyocyte proliferation by targeting a network of negative cell-cycle regulators (Raso et al., 2021). Pregnancy-specific studies have also implicated miR-25-3p in trophoblast-to-myometrium sEV signaling, suggesting a possible role in regulating uterine contractility and the timing of labor (Wang et al., 2021). These mechanistic insights may suggest that positive association of miR-25-3p in response to prenatal BC could be a compensatory mechanism to counteract pollution-induced stress (by preventing apoptosis and sustaining cell proliferation). Similarly, miR-433-3p (positive association with BC) has been shown to inhibit neuronal cell growth while promoting autophagy in experimental models (Xu et al., 2020). Higher cord-blood EV miR-433-3p may be consistent with reduced neuronal proliferation or increased autophagy-related signaling during neurodevelopment, although this remains speculative because tissue origin and functional consequences were not directly assessed.

Perhaps most intriguing is the negative association of the placenta-specific C19MC microRNAs (miR-518a-3p and miR-519a/b-3p) in relation to BC. Members of the C19MC cluster are almost exclusively expressed in the placenta and packaged into EVs that communicate with maternal and fetal tissues (Xu et al., 2021). Our results suggest that higher fetal BC burdens correlate with lower levels of these placenta-derived miRNAs in fetal circulation. This is in line with a recent report that ambient PM exposure can alter EV-miRNA profiles derived from the placenta (Tsamou et al., 2018). MiR-519a and related C19MC miRNAs have been implicated in placental development and pregnancy complications (Wang et al., 2014; Cao et al., 2025). For example, miR-519a is reported to be reduced in cases of intrauterine growth restriction, and miR-519d (another C19MC member) is elevated in pre-eclampsia placentas (Cao et al., 2025). Although miR-518a-3p and miR-519a/b did not show placenta development pathways in single-miRNA enrichment (likely due to limited annotation of their targets), the combined analysis did reveal placenta development as a significantly enriched process (FDR <0.001). It is plausible that BC particles deposited in the placenta (Bové et al., 2019) induce local oxidative stress or inflammatory responses that suppress the expression or release of these trophoblast-derived miRNAs (Ferrari et al., 2022). A reduction in placenta-enriched miRNAs could disturb normal placental signaling to the fetus, potentially affecting nutrient transport or immunological balance at the maternal-fetal interface. This finding provides a novel molecular insight that placental miRNA communication is sensitive to pollution exposure, and it complements earlier DNA methylation studies showing placental epigenetic changes associated with air pollution (Klibaner-Schiff et al., 2025).

MiR-520g-3p/520h, which was negatively associated with BC (FDR $= 0.079$), is encoded adjacent to the C19MC cluster and shares evolutionary and functional links with other C19MC members (Malnou et al., 2019). Its suppression in high-BC cord blood adds to the evidence that this genomic locus is sensitive to particulate matter exposure. Per-miRNA target enrichment revealed involvement in hematopoietic and cardiac developmental pathways, including myeloid cell differentiation and heart development, which are distinct from the predominantly neurodevelopmental profiles of miR-25-3p, miR-433-3p, and miR-519a-3p/519b-3p. This suggests that different BC-responsive miRNAs may perturb complementary aspects of fetal development. MiR-520g-3p has been reported to regulate trophoblast invasion and placental function (Mouillet et al., 2025), and its downregulation in response to BC could therefore contribute to placental dysfunction alongside the suppression of miR-518a-3p and miR-519a/b.

The biological significance of these miRNA changes is supported by the enrichment of developmentally relevant pathways among their gene targets. The strong over-representation of neurodevelopmental pathways (axon guidance, synaptic signaling, neurotrophic support) in our analysis resonates with growing evidence that prenatal air pollution can impair neurodevelopment, manifesting as behavioral and cognitive deficits in childhood (Wang et al., 2022). It is noteworthy that BC particles have been observed on the fetal side of the placenta (Bové et al., 2019) and even in fetal organs (Bongaerts et al., 2022), including the developing brain. Ultrafine particles like BC or magnetite can cross the blood-brain barrier (Maher et al., 2016); for instance, magnetite nanoparticles from air pollution have been detected in human brain tissue, where they may generate oxidative stress. Such direct fetal brain exposure could trigger molecular responses, possibly including altered miRNA expression, that perturb neurodevelopmental processes. Our finding that BC-associated miRNAs target genes involved in neuron projection and synapse formation hints at one mechanism by which maternal inhalational exposures might translate into altered brain development in early life.

From a mechanistic standpoint, our results support the concept that EVs and their miRNA cargo are active responders to environmental exposures. Short-term exposure studies in adults have shown that particulate pollutants can alter circulating EV concentrations and miRNA content (Bonzini et al., 2017; Pergoli et al., 2017). Here we extend this paradigm to the prenatal setting, with evidence that the EV-miRNA profile in the fetus shifts in relation to a specific internalized pollutant (BC). EVs could facilitate cross-placental communication of stress signals: maternal inhalation of pollutants may induce placental inflammation, leading the placenta to release EVs with a distinct miRNA profile into the fetal circulation (Ferrari et al., 2022). Those EV-miRNAs might then modulate gene expression in fetal organs (e.g., suppressing or enhancing certain developmental pathways). Additionally, some EVs in cord blood are of fetal origin, so fetal tissues directly impacted by BC (such as the fetal liver or lungs) could also release miRNA-rich EVs as part of their response. The net effect is a circulating miRNA signal in the fetus that mirrors the exposure-related disturbances in both placenta and fetal tissues. Our identification of specific miRNAs and pathways

provides candidate molecular mediators for future functional studies. For example, *in vitro* experiments could test whether BC exposure to trophoblast cells causes down-regulation of C19MC miRNAs and whether that in turn affects angiogenic signaling in endothelial cells.

Our study has several strengths, including the use of a well-characterized birth cohort, direct quantification of cord-blood BC as an internal exposure biomarker, and profiling of EV-associated miRNAs in a biologically informative circulating compartment characterized according to current EV reporting recommendations. However, several limitations should also be considered. First, the observational design precludes definitive conclusions about causality. While we adjusted for key confounders (infant sex, maternal ethnicity, maternal age, and sequencing batch), unmeasured factors (e.g., maternal nutrition, psychosocial stress, or co-exposures like other pollutants) could also influence EV-miRNA profiles. In addition, some pregnancy-related and socioeconomic variables, including gestational age and detailed obstetric complications, were not available with sufficient completeness and reliability in the molecular substudy dataset, partly because sampling and data extraction overlapped with the COVID-19 period. We therefore avoided using these incomplete variables for descriptive comparison or covariate adjustment. Our sample size ($N = 68$ for miRNA-BC analyses) provided adequate power to detect moderate associations but may have missed smaller effect sizes; replication in larger cohorts is warranted. A further statistical limitation is that the per-miRNA association models were fitted after elastic-net candidate selection. Consequently, the reported p-values are post-selection p-values and should not be interpreted as confirmatory evidence. We therefore interpret the results based on consistency of effect direction, nominal association strength, detection frequency, biological coherence, and holdout stability, with replication in independent cohorts required. Another limitation is the reliance on validated target databases and enrichment analysis to infer function. Not all miRNA targets are known, especially for placenta-specific miRNAs, and target repression can be context-dependent. Therefore, the pathway enrichments serve as hypotheses rather than direct proof of biological effect. We also cannot pinpoint which tissue(s) produce the altered EV-miRNAs, placenta is a likely source for some (given C19MC origin), whereas others (miR-25, etc.) might derive from fetal endothelial cells or blood cells. Future studies using cell-specific EV markers or placental perfusion models could clarify the origin of these signals. Additionally, our EV isolation (polymer precipitation + SEC) yields a heterogeneous mix of small EVs; although we confirmed the presence of exosomes by markers, we cannot exclude co-isolation of other particle types (which might carry miRNAs as well). We did not directly quantify depletion of common non-vesicular contaminants or negative markers, such as lipoproteins, albumin, ApoA1/ApoB, or calnexin. Therefore, although NTA, cryo-TEM, and canonical EV markers support an EV-enriched preparation, we cannot exclude co-isolation of lipoprotein particles, protein complexes, or other extracellular RNA carriers. The findings should therefore be interpreted as sEV-enriched extracellular miRNA signals rather than pure exosome-specific cargo. Technical variability in small RNA sequencing and the low RNA input could also influence miRNA detection, though we implemented rigorous QC and a validation via holdout resampling to ensure robust results. Finally, because this analysis was cross-sectional at birth, the long-term consequences of the observed miRNA differences remain unknown. It will be important to follow up whether newborns with higher BC and altered EV-miRNA profiles go on to experience differences in growth, neurodevelopment, or other health outcomes.

In conclusion, our study provides novel evidence that maternal exposure to combustion-derived particulate matter is associated with shifts in EV-encapsulated microRNA profiles established in cord blood, with the affected miRNAs targeting genes in key developmental pathways. These EV-miRNA biomarkers may reflect early-life epigenetic regulation changes, offering insight into how the intrauterine environment shapes child health. The identification of specific miRNAs (e.g., miR-25-3p, miR-433-3p, miR-518a-3p, miR-519a/b-3p, miR-520g-3p/520h) linking prenatal air pollution to biological processes like neurogenesis and angiogenesis is particularly compelling. It suggests a mechanistic framework whereby inhaled pollutants, after crossing into fetal circulation, can modify gene regulatory circuits via miRNAs, potentially leading to "epigenetic reprogramming" of development. This finding reinforces the urgency of reducing maternal pollution exposures as a preventive strategy. Moreover, EV-derived miRNAs could serve as accessible biomarkers of fetal exposure and effect: measuring these miRNAs in cord blood might help identify infants at higher risk of pollution-related complications, enabling early interventions. As air quality continues to be a pressing global health issue, understanding and mitigating the impact of air pollution on the most vulnerable (unborn children) should be a high research priority. Our results lay the groundwork for future mechanistic studies, replication in independent cohorts, and longitudinal follow-up to determine whether these EV-miRNA signatures predict later health outcomes. They also support continued efforts to reduce maternal exposure to combustion-related air pollution through public health and policy measures.

These discoveries contribute to the growing field of environmental epigenetics and emphasize that the seeds of adult disease may be sown through subtle miRNA-mediated shifts *in utero*. Future research integrating multi-omics approaches and longitudinal follow-up will further elucidate how early-life exposure translates into later-life health and whether interventions (such as improved maternal nutrition or antioxidant therapies) can modulate these miRNA responses for better outcomes. Ultimately, our findings underscore that improving air quality is not only crucial for the environment but is also fundamentally an investment in the health of the next generation.

Declaration of generative AI and AI-assisted technologies in the writing process

We have not used AI-assisted technologies to create this article.

Funding

This study was supported by Children with Cancer UK (Grant Reference 19 - 311).

CRediT authorship contribution statement

Houman Kahroba: Conceptualization, Data curation, Formal analysis, Investigation, Methodology, Resources, Software, Validation, Visualization, Writing – original draft, Writing – review & editing. **Kenneth Vanbrabant:** Data curation, Formal analysis. **Marcel van Herwijnen:** Data curation, Methodology. **Rick Kamps:** Data curation. **Matthew Walker:** Data curation, Resources. **Dagmar Waiblinger:** Data curation, Resources. **Marcel Ameloot:** Formal analysis, Methodology, Writing – review & editing. **Michelle Plusquin:** Resources, Supervision, Writing – review & editing. **John Wright:** Conceptualization, Funding acquisition, Resources, Writing – review & editing. **Tim Nawrot:** Conceptualization, Funding acquisition, Methodology, Resources, Supervision, Writing – review & editing. **Theo M. de Kok:** Conceptualization, Funding acquisition, Methodology, Resources, Supervision, Writing – review & editing. **Julian Krauskopf:** Conceptualization, Formal analysis, Funding acquisition, Methodology, Supervision, Validation, Writing – review & editing.

Declaration of competing interest

The authors declare that they have no known competing financial interests or personal relationships that could have appeared to influence the work reported in this paper.

Acknowledgements

We thank Children with Cancer UK (Grant Reference 19 - 311) for their financial support of the project.

Appendix A. Supplementary data

Supplementary data to this article can be found online at https://doi.org/10.1016/j.envres.2026.125159.

Data availability

Data will be made available on request.

References

Alisch, R.S., Jin, P., Epstein, M., Caspary, T., Warren, S.T., 2007. Argonaute2 is essential for mammalian gastrulation and proper mesoderm formation. PLoS Genet. 3, 2565–2571.
Bernstein, E., et al., 2003. Dicer is essential for mouse development. Nat. Genet. 35, 215–217.
Bongaerts, E., et al., 2022. Maternal exposure to ambient black carbon particles and their presence in maternal and fetal circulation and organs: an analysis of two independent population-based observational studies. Lancet. Planet. Heal. 6, e804.
Bonzini, M., et al., 2017. Short-term particulate matter exposure induces extracellular vesicle release in overweight subjects. Environ. Res. 155, 228–234.
Bové, H., et al., 2016. Biocompatible label-free detection of carbon black particles by femtosecond pulsed laser microscopy. Nano Lett. 16, 3173–3178.
Bové, H., et al., 2019. Ambient black carbon particles reach the fetal side of human placenta. Nat. Commun. 10.
Bridges, S., et al., 2025. Born and Bred in (BaBi): an efficient, place-based birth e-cohort network. NIHR Open Res. (5), 66, 2025 566.
Cao, S.Q., Jiang, T.X., Guo, Y.Y., Lin, R., Lin, L., 2025. MiR-519d-3p from placenta-derived exosomes induce immune intolerance regulating immune cells, contributing to the pathogenesis of Preeclampsia. Immunol. Investig. 54, 522–543.
Chandrasekera, D., et al., 2023. Combination of precipitation and size exclusion chromatography as an effective method for exosome like extracellular vesicle isolation from pericardial fluids. Nanotheranostics 7, 345.
Concepcion, C.P., Bonetti, C., Ventura, A., 2012. The miR-17-92 family of microRNA clusters in development and disease. Cancer J. 18, 262.
Dickerson, J., et al., 2022. Born in Bradford's Better Start (BiBBS) interventional birth cohort study: interim cohort profile. Wellcome Open Res. 7, 244.
Donker, R.B., et al., 2012. The expression profile of C19MC microRNAs in primary human trophoblast cells and exosomes. Mol. Hum. Reprod. 18, 417–424.
Ferrari, L., et al., 2022. Extracellular vesicles and their miRNA contents counterbalance the pro-inflammatory effect of air pollution during physiological pregnancy: a focus on Syncytin-1 positive vesicles. Environ. Int. 169, 107502.
Foley, H.B., et al., 2024. EV-miRNA Associated with Environmental Air Pollution Exposures in the MADRES Cohort, 10.
Ilekis, J.V., et al., 2016. Placental origins of adverse pregnancy outcomes: potential molecular targets: an executive workshop summary of the Eunice Kennedy Shriver national institute of child health and human development. Am. J. Obstet. Gynecol. 215, S1–S46.
Janssen, N.A.H., et al., 2011. Black carbon as an additional indicator of the adverse health effects of airborne particles compared with PM10 and PM2.5. Environ. Health Perspect. 119, 1691–1699.
Ji, N., et al., 2023. Prenatal ambient air pollution exposure and child weight trajectories from the 3rd trimester of pregnancy to 2 years of age: a cohort study. BMC Med. 21, 341, 2023 *211*.
Jin, K., Shen, S., Shi, R., Xu, X., Hu, M., 2024. Exosomal miRNAs in prenatal diagnosis: recent advances. Medicine (Baltim.) 103, e38717.
Kahroba, H., et al., 2025. Small Extracellular Vesicles: Connecting Early Life Exposure Outcomes to Air Pollution During Pregnancy to Early Childhood Health, 24.
Klibaner-Schiff, E., et al., 2025. Distinct DNA methylation in mother-infant dyads exposed to PM2.5 in pregnancy. Clin. Epigenet. 17, 197, 2025 171.
Love, M.I., Huber, W., Anders, S., 2014. Moderated estimation of fold change and dispersion for RNA-seq data with DESeq2. Genome Biol. 15, 1–21, 2014 *1512*.
Lu, Y., Thomson, J.M., Wong, H.Y.F., Hammond, S.M., Hogan, B.L.M., 2007. Transgenic over-expression of the microRNA miR-17-92 cluster promotes proliferation and inhibits differentiation of lung epithelial progenitor cells. Dev. Biol. 310, 442–453.
Maher, B.A., et al., 2016. Magnetite pollution nanoparticles in the human brain. Proc. Natl. Acad. Sci. U. S. A. 113, 10797–10801.
Malnou, E.C., Umlauf, D., Mouysset, M., Cavaillé, J., 2019. Imprinted MicroRNA gene clusters in the evolution, development, and functions of Mammalian placenta. Front. Genet. 9, 706.
Mouillet, J.F., et al., 2025. The Chromosome 19 miRNA cluster guards trophoblasts against overacting innate immunity. Commun. Biol. 8, 1511, 2025 81.
Niranjan, R., Thakur, A.K., 2017. The toxicological mechanisms of environmental soot (black carbon) and carbon black: focus on Oxidative stress and inflammatory pathways. Front. Immunol. 8, 763.
Ouyang, Y., Mouillet, J.F., Coyne, C.B., Sadovsky, Y., 2013. Placenta-specific microRNAs in exosomes – good things come in nano-packages. Placenta 35 (Suppl. l), S69.
Pergoli, L., et al., 2017. Extracellular vesicle-packaged miRNA release after short-term exposure to particulate matter is associated with increased coagulation. Part. Fibre Toxicol. 14, 32.
Pope, C.A., et al., 2006. Health effects of fine particulate air pollution: lines that connect. J. Air Waste Manag. Assoc. 56, 1368–1380.
Raso, A., et al., 2021. A microRNA program regulates the balance between cardiomyocyte hyperplasia and hypertrophy and stimulates cardiac regeneration. Nat. Commun. 12, 4808, 2021 *121*.
Rodosthenous, R.S., et al., 2015. Ambient particulate matter and {microRNAs} in extracellular vesicles: a pilot study of older individuals. Part. Fibre Toxicol. 13.
Saenen, N.D., et al., 2017. Children's urinary environmental carbon load: a novel marker reflecting residential ambient air pollution exposure? Am. J. Respir. Crit. Care Med. 196, 873–881.
Suh, N., et al., 2010. MicroRNA function is globally suppressed in mouse oocytes and early embryos. Curr. Biol. 20, 271–277.
Tsamou, M., et al., 2018. Air pollution-induced placental epigenetic alterations in early life: a candidate miRNA approach. Epigenetics 13, 135–146.
Tsamou, M., et al., 2020. Prenatal particulate air pollution exposure and expression of the miR-17/92 cluster in cord blood: findings from the ENVIRONAGE birth cohort. Environ. Int. 142, 105860.
Wang, D., Na, Q., Song, W.W., Song, G.Y., 2014. Altered expression of miR-518b and miR-519a in the placenta is associated with low fetal birth weight. Am. J. Perinatol. 31, 729–734.
Wang, J., et al., 2023. Systematic assessment of small RNA profiling in human extracellular vesicles. Cancers (Basel) 15, 3446.
Wang, L., Zhang, W., Zou, N., Zhang, L., 2021. Trophoblasts modulate the Ca2+ oscillation and contraction of myometrial smooth muscle cells by small extracellular Vesicle- (sEV-) mediated exporting of miR-25-3p during premature labor. Oxid. Med. Cell. Longev. 2021, 8140667.
Wang, P., et al., 2022. Prenatal fine particulate matter exposure associated with placental small extracellular vesicle derived microRNA and child neurodevelopmental delays. Sci. Total Environ. 841.
Welsh, J.A., et al., 2024. Minimal information for studies of extracellular vesicles (MISEV2023): from basic to advanced approaches. J. Extracell. Vesicles 13.
Xu, C., et al., 2020. miR-433 inhibits neuronal growth and promotes autophagy in Mouse Hippocampal HT-22 cell line. Front. Pharmacol. 11, 536913.
Xu, P., Ma, Y., Wu, H., Wang, Y.L., 2021. Placenta-Derived MicroRNAs in the Pathophysiology of Human Pregnancy, 9, 646326.